Applied Catalysis A, General 670 (2024) 119541

Contents lists available at ScienceDirect

Applied Catalysis A, General

journal homepage: www.elsevier.com/locate/apcata

The application of alumina supported Pd catalysts for high selectivity aniline synthesis catalysis at elevated temperatures: Site-selective chemistry

J.W. Campbell [a], A.M. McCullagh [a], L. McGrath [a], C. How [b], D.A. MacLaren [b], M. Loenders [c], N. Meyer [c], R.H. Carr [c], D. Lennon [a,*,1]

[a] School of Chemistry, Joseph Black Building, University of Glasgow, Glasgow G12 8QQ, UK
[b] School of Physics and Astronomy, Kelvin Building, University of Glasgow, Glasgow G12 8QQ, UK
[c] Huntsman Polyurethanes, Everslaan 45, 3078 Everberg, Belgium

ARTICLE INFO

Keywords:
Nitrobenzene hydrogenation
Aniline synthesis catalysis
Pd/Al_2O_3 catalyst
Site-selective chemistry
Infrared spectroscopy

ABSTRACT

The industrial scale heterogeneously catalysed hydrogenation of nitrobenzene to produce aniline is ideally suited to the incorporation of heat recovery strategies. However, a range of by-products may be observed. Thus, discerning the origins of by-product formation is crucial for developing targeted prototype catalysts. This paper examines by-product formation at elevated reaction temperatures over a previously untested low loading alumina-supported Pd (0.3 wt%) industrial grade prototype aniline synthesis catalyst in the vapour and liquid phase. Infrared spectroscopy of chemisorbed CO is used to evaluate the Pd crystallite morphology. Importantly, the morphology is seen to differ from other previously analysed 0.3 wt% Pd/Al_2O_3 catalyst samples. Post-reaction (vapour phase) analysis of the catalyst identifies carbon laydown to preferentially neutralise Pd(100) sites. An inter-relationship is proposed *via* observed nitrobenzene hydrogenation chemistry and crystallite morphology, such that specific reactions are associated with specific planes of the Pd crystallites of this Pd/Al_2O_3 catalyst.

1. Introduction

Nitrobenzene hydrogenation is employed in the production of aniline, a crucial chemical utilised in the polyurethane industry to produce methylene diphenyl diisocyanate (MDI) [1]. This paper is entrenched in the application of infrared (IR) spectroscopy to ascertain an interrelationship between catalytic activity and metal crystallite morphology of a high aniline selectivity industrial prototype Pd/Al_2O_3 catalyst and represents the culmination of a significant work package concerning the hydrogenation of nitrobenzene with such catalysts [2–5]. The body of work is connected to the implementation of performing the reaction at elevated temperatures to optimise heat recovery options at the industrial complex [3].

High selectivity aniline synthesis has been reported for a range of metal supported heterogeneous catalysts. Corma et al. investigated the liquid phase hydrogenation of nitrobenzene in a batch reactor utilising a Au/TiO_2 catalyst [6]. Selective aniline formation was achieved (*ca.* 95%); however, nitrobenzene conversion remained comparitively low at *ca.* 40%. This is associated with the lessened ability of Au catalysts to dissociatively adsorb hydrogen [7]. Another liquid phase study by Zhang and co-workers probed nitrobenzene hydrogenation with Pt/CeO_2 utilising a variety of CeO_2 support shapes [8]. A maximum aniline yield was reported for Pt supported on rod-shaped CeO_2 which corresponded to 100% nitrobenzene conversion and 87.2% aniline selectivity. Ni supported catalysts also exhibit good aniline selectivity. For example, Wang et al. report an investigation of nitrobenzene hydrogenation to aniline utilising Ni/SiO_2 [9]; at a reaction temperature of 70 °C complete reagent conversion was noted after 4.0 h associated with an aniline selectivity of 83.5%. Interestingly, additional sampling after 5.5 h Time-on-Stream (T-o-S) showed an increase in aniline selectivity to 98.7%, perhaps indicating an element of product retention to the catalyst at 4.0 h. More pertinent to the present investigation, Pd supported catalysts also permit high selectivity aniline synthesis from the hydrogenation of nitrobenzene. For example, Sá Couto et al. report a

* Corresponding author.
E-mail address: David.Lennon@glasgow.ac.uk (D. Lennon).
[1] School of Chemistry, Joseph Black Building, The University of Glasgow, Glasgow, G12 8QQ, U.K.

https://doi.org/10.1016/j.apcata.2023.119541
Received 2 October 2023; Received in revised form 3 December 2023; Accepted 11 December 2023
Available online 13 December 2023

parametric investigation of the liquid phase nitrobenzene hydrogenation at 120 °C in a tubular fixed-bed reactor using a commercial Pd/Al_2O_3 catalyst [10]. Here, reagent conversion was observed to independently increase as a function of increasing temperature and pressure, whilst aniline selectivity decreased, owed to the increased formation of secondary by-products. Parameters (temperature, pressure and nitrobenzene concentration in aniline) were varied at separate points throughout the same reaction. Consideration of the full data set as a function of T-o-S indicated retainment of near complete nitrobenzene conversion throughout and an increase in aniline selectivity to *ca.* 99% from 80 h onwards. Thus, high aniline synthesis catalysis is permissible with a variety of metal supported catalysts.

Concentrating on low loading Pd/Al_2O_3 catalysts, the authors have previously used a combination of reference and industrial grade Pd/Al_2O_3 catalysts to discern a global reaction scheme (Scheme 1) [4] that accounts for majority product formation as well as a surprisingly wide range of by-products. With reference to Scheme 1, the main transformation of nitrobenzene hydrogenation to aniline is highly selective and is reported to occur *via* a phenylhydroxylamine (PHA) intermediate [11,12]. By-product production can then be split into 4 separate pathways. Firstly, pathway-1 derives from hydrogenation of the product (aniline) to yield cyclohexylamine (CHA); CHA then couples with aniline to produce N-cyclohexylaniline (CHAN) and a subsequent hydrogenation gives dicyclohexylamine (DICHA). Pathway-1 is assigned as the dominant route to reduced aniline selectivity [3,4]. Pathway-2 arises from nitrobenzene derived intermediates and produces cyclohexanone oxime (CHOX), with hydrolysis yielding cyclohexanone (CHO) and hydrogenation giving cyclohexanol (CHOL). The chemistry associated with pathway-3 is established [11,12] and involves coupling of nitrobenzene intermediates to yield azoxybenzene (AZOXY), azobenzene (AZO) and hydrazobenzene (HYDRAZO), which provide a condensation route to aniline. Finally, pathway-4 is, again, associated with nitrobenzene

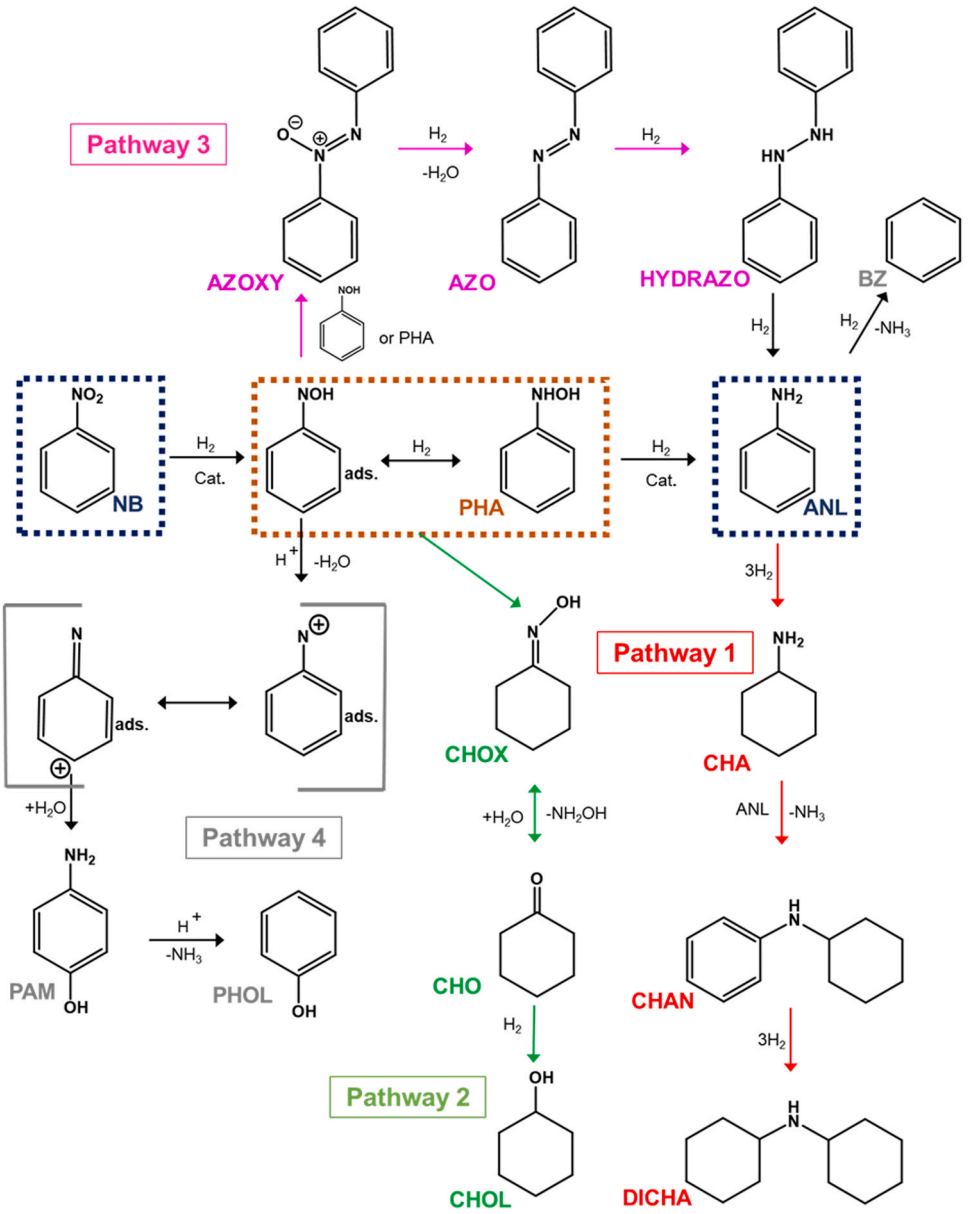

Scheme 1. Scheme for nitrobenzene (NB) hydrogenation to aniline (ANL) *via* a phenylhydroxylamine intermediate (PHA) in the vapour phase depicting 4 pathways to by-product formation. Pathway 1 by-products (red): cyclohexylamine (CHA), N-cyclohexylaniline (CHAN) and dicyclohexylamine (DICHA). Pathway 2 by-products (green): cyclohexanone oxime (CHOX), cyclohexanone (CHO) and cyclohexanol (CHOL). Pathway 3 by-products (purple): azoxybenzene (AZOXY), azobenzene (AZO) and hydrazobenzene (HYDRAZO). Pathway 4 by-products (grey): para-aminophenol (PAM) and phenol (PHOL). The scheme is reproduced from Reference 4 with permission from the American Chemical Society (link: <https://pubs.acs.org/doi/10.1021/acs.iecr.2c01134>).

derived intermediates leading to the formation of a series of surface bonded nitrenium ions. From this para-aminophenol (PAM) and phenol (PHOL) are accessible [4]. Fig. S1 presents the abbreviations used to describe the molecules considered within Scheme 1 and that feature within the forthcoming discussion.

Against this background of understanding concerning nitrobenzene hydrogenation over a range of Pd/Al_2O_3 catalysts, this article examines a new 0.3 wt% Pd/Al_2O_3 catalyst not previously investigated by the authors and classified herewith as GU-6. Table S1 (Supporting Information section) describes the six Pd/Al_2O_3 catalysts examined as part of this medium-range academic/industrial collaboration. GU-6 is a technical grade catalyst supplied by Huntsman Polyurethanes that is comparable to two other 0.3 wt% Pd/Al_2O_3 catalysts investigated previously (GU-2 [3] and GU-4 [4]) but it is highlighted here as it exhibits sustained and elevated aniline yields. Thus, its examination in the context of Scheme 1 provides the opportunity to develop a structure/activity relationship for the Pd crystallites of this material. Reaction testing is undertaken at high nitrobenzene conversions, as encountered in the industrial operation, with the central theme of the investigation being to correlate by-product formation with catalyst characteristics under conditions of elevated temperature that favour new heat recovery strategies [3].

The paper is comprised as follows. The morphology of the Pd nanoparticles of GU-6 is determined by a combination of CO chemisorption and temperature-programmed infrared spectroscopy (TP-IR). Reaction testing in the vapour phase establishes high aniline selectivity to be maintained as, *via* a deactivation process, the conversion asymptotes to a fixed value. Over a 25 h period, liquid phase testing additionally returns elevated aniline yields. Post-reaction (vapour phase) catalyst characterisation by IR spectroscopy reveals the selective poisoning of Pd(100) facets, which are linked to by-products associated with Pathway 1. These outcomes represent an example of site-selective chemistry, with a particular facet of the Pd crystallites responsible for a discrete by-product sequence. Such outcomes bring us closer to linking catalyst specification to defined reaction profiles. In this case, the formation of a compound (aniline) that forms part of a large-scale chemical manufacturing product chain (isocyanates).

2. Experimental

The catalyst is a 0.3 wt% Pd/Al_2O_3 egg-shell type catalyst (pellets = 2.4 – 1.7 mm), supplied by Huntsman Polyurethanes, which represents an industrial prototype for nitrobenzene hydrogenation. The catalyst was ground to a powder (500 – 250 μm) for catalyst characterisation and reaction testing, unless otherwise stated. The catalyst will be referred to as GU-6. For comparison, Table S1 classifies the other five Pd/Al_2O_3 catalysts examined as part of the overall study into aniline synthesis catalysis.

2.1. Catalyst characterisation

2.1.1. CO chemisorption, AAS, BET and TEM

CO chemisorption, atomic absorption spectrophotometry (AAS), Brunner-Emmett-Teller (BET) and Transmission Electron Microscopy (TEM) measurements of GU-6 were performed as detailed in reference [3]. Briefly, CO adsorption isotherms were obtained at 298 K using a pulse-flow method utilising an in-line gas chromatograph (Thermo Finnigan, Trace GC, TCD detector). Palladium loading was measured by AAS by means of a Perkin Elmer Analyst 100 instrument ($\lambda = 244.8$ nm). BET total surface area measurements were carried out on a Micromeritics ASAP 2400 gas adsorption analyser using a static barometric method. TEM was performed on a Tecnai T20 microscope with an accelerating voltage of 200 keV. Additional post reaction BET and TEM measurements were taken after nitrobenzene hydrogenation (conditions as stated in Section 2.2.1) after 135 h time-on-stream.

2.1.2. CO temperature-programmed IR spectroscopy

Diffuse reflectance infrared Fourier Transform spectroscopy (DRIFTS) was performed *in situ* and involved a sample handing stage. Scrapings of the outer layer of the pelleted catalyst were utilised. This method for CO TP-IR measurement of a low loading metal catalyst has been reported in reference [3] and has been duplicated here. To facilitate application of the "scraping technique" detailed above, post-reaction CO TP-IR measurements are associated with reaction testing performed with pelleted GU-6.

2.2. Reaction testing

2.2.1. Vapour phase

Reaction testing was carried out in the vapour phase over a period of up to 120 h using a plug flow reactor (¼" stainless steel, internal diameter: 0.18") arrangement housed in a split tube furnace (LPC Elements) at a reaction temperature of 160 °C. H_2 (25 mL min^{-1}; BOC gases, 99.8%) and He (12.5 mL min^{-1}; BOC gases, 99.9%) were supplied by mass flow controllers (Brooks, 5850 TR series). Nitrobenzene was supplied as a vapour using a heated bubbler system that delivered 1.44 $\mu mol_{(NB)}$ min^{-1}. The nitrobenzene was premixed with hydrogen to a give a H_2:$C_6H_5NO_2$ molar flow ratio of *ca.* 600:1. Catalyst reduction (temperature: 200 °C; H_2:He flow = 15:35 mL min^{-1}) and reaction sampling was performed as described in reference [4]. As noted previously [3], the large hydrogen excess was selected to expose the accessibility of all hydrogenation pathways illustrated in Scheme 1. There was no catalyst conditioning period deployed in these studies.

Reaction testing data sets contained herewith correspond to nitrobenzene hydrogenation with powdered GU-6 (500 – 250 μm). Additional nitrobenzene hydrogenation with pelleted GU-6 was performed with the same reaction conditions to permit post-reaction CO TP-IR measurements (Section 2.1.1). Post-reaction, the catalyst was regenerated utilising a temperature ramp (5 °C min^{-1}) up to a temperature of 330 °C and a H_2/He flow of 15/35 mL min^{-1}. Reaction testing was then conducted exactly as described for the fresh catalyst.

Nitrobenzene conversion was calculated according to Eq. 1 [13],

$$\mathrm{Conv.NB}(\%) = \frac{\mathrm{nNB}(0) - \mathrm{nNB}(t)}{\mathrm{nNB}(0)} \times 100 \quad (1)$$

where $n\mathrm{NB}(0)$ represents the initial number of moles of nitrobenzene and $n\mathrm{NB}(t)$ the number of moles of nitrobenzene at time t. Product selectivity values were calculated according to Eq. 2 [13],

$$\mathrm{Select.X}(\%) = \frac{\mathrm{nX}(t)}{\mathrm{ntotal}(t) - \mathrm{nNB}(t)} \times 100 \quad (2)$$

where $n\mathrm{X}(t)$ represents the number of moles of compound X at time t and $n\mathrm{total}(t)$ the total number of moles of all observed compounds at time t. Aniline yield values were calculated according to Eq. 3 [13].

$$\mathrm{Yield.ANL}(\%) = \frac{\mathrm{Conv.NB}(t) \times \mathrm{Select.ANL}(t)}{100} \quad (3)$$

where $Conv.NB(t)$ represents percent nitrobenzene conversion at time t and $Select.ANL(t)$ the percent selectivity of aniline at time t. Weight hourly space velocity (WHSV) values, defined as the mass of nitrobenzene normalised to catalyst mass per unit time [14–16], were calculated according to Eq. 4,

$$\mathrm{WHSV}\left(h^{-1}\right) = \frac{m_{NB} \quad h^{-1}}{m_{cat.}} \quad (4)$$

where $m_{NB} \quad h^{-1}$ represents the mass of the nitrobenzene per hour and $m_{cat.}$ catalyst mass.

2.2.2. Liquid phase

Liquid phase experiments were performed using a continuous flow

micro reactor suitable for studying catalytic hydrogenation of nitrobenzene to aniline in a tubular fixed bed reactor (I.D.: 16.5 mm), designed for down-flow trickle bed operation. A schematic illustration of the reactor set up is presented in the Supporting Information (Fig. S2). The reactor is housed in a single zone split furnace and a uniform and isothermal temperature profile was obtained in the middle section of the reactor. The first 8 cm of the reactor tube was filled with glass beads (diameter: 3 mm), followed by 8 cm of coarse SiC (2.4 – 1.7 mm) and then 2.5 cm of fine SiC powder (500 – 355 μm). The mid-section of the reactor was loaded with 4 g of GU-6 in pellet form (trilobe shape, 2.5 mm) in three separate aliquots, with an addition of a small quantity of fine SiC between each aliquot. This provided a mixed bed length of *ca.* 3.5 – 4 cm in the middle of the reactor. On top of the mixed catalyst bed a further volume of fine silicon carbide was added (3 cm length) and a further 8 cm depth of coarse silicon carbide. The loading of the catalyst with the two grades of silicon carbide fulfils several objectives. Firstly, the contact of the liquid feed with the catalyst particles is maximised. Secondly, the presence of the fine silicon carbide particles determines the overall liquid hydrodynamics within the bed, allowing more reproducible and scalable results to be obtained. Finally, silicon carbide has a high thermal conductivity compared with glass or other inert materials, and therefore the magnitude of any thermal gradients within the reactor tube will be reduced.

Catalyst activation was done by flushing the reactor tube with nitrogen at 30 NL h^{-1} for 10 min. Hydrogen (99.999% purity) was then fed to the unit at 30 NL h^{-1} whilst the temperature was increased to 265 °C (approximately 30 min). Gases were controlled by gas flow controllers (Brooks 5850). During this period the reactor back pressure valve was kept open to ensure a good hydrogen flow through the unit. After the catalyst activation step was complete the back pressure valve was adjusted to build up pressure in the unit. The hydrogen flow rate was kept at 30 NL h^{-1} until a pressure of 20 barg was achieved (approximately 20 min).

For the hydrogenation reaction, water (0.5 mL min^{-1}) and 14% w/w nitrobenzene in aniline (1.0 mL min^{-1}) were pumped into the reactor unit by HPLC pumps (Gibson 305 piston pumps with Gibson 807 manometric module for the water side and Gibson 806 for the NB/ANL side). A hydrogen flow of 6.2 NL h^{-1} was utilised for reaction testing (Conditions: temp. – 265 °C; pressure: 20 barg). The inclusion of product alongside the reactant mimics a revised process operation stage that relates to improved heat recovery performance in a version of the large-scale unit operation [17].

The effluent from the reactor was passed through an air-cooled coil and led into a high-pressure gas-liquid separator. The liquid level was controlled by a capacitive level transmitter that controls the opening/closing of the pneumatic Kammer valve for the draining of the liquid. Samples were taken from the unit at regular time intervals. The liquid reactor samples were analysed using an Agilent Technologies 6850 GC-system fitted with a 7683 B Series Injector and a FID detector. The GC-system was calibrated with standard chemicals purchased from Aldrich. Due to restricted access, reaction testing data is only available for a period of 24 h.

2.3. Temperature-programmed oxidation

Temperature-programmed oxidation (TPO) measurements were carried out post-nitrobenzene hydrogenation (vapour phase, conditions as stated in Section 2.2.1.) for a set time-length (1, 12, 21.5, 43, 66 and 96 h). Thereafter, the reactor was cooled in flowing He (68.8 mL min^{-1}) for *ca.* 3 h. A 5% O_2/He flow (20 mL min^{-1}; BOC Gasses, 99.8%) was introduced over GU-6 and the reactor was heated to 600 °C under a temperature ramp (15 °C min^{-1}). Oxidation product CO_2 was monitored *via* mass spectrometry (MKS Microvison Plus).

3. Results

3.1. Catalyst characterisation: pre-reaction

3.1.1. CO chemisorption, AAS, BET and TEM

Catalyst characterisation measurements for the as received GU-6 sample are surmised in Table 1. A palladium loading of 0.38 wt% was determined for the catalyst, amounting to 26.6% more Pd than the 0.3 wt% nominal loading. BET derived total surface area was 119.6 ± 3.59 m^2 g^{-1}. The reduced sample achieved a saturation coverage of CO of 10.0 μmol CO $g^{-1}_{(cat)}$, from which a catalyst dispersion of 70.8% and mean Pd particle size of 1.54 nm were derived assuming a CO: Pd(s) stoichiometry of 1:2 [18].

Analysis of TEM micrographs of the as-received GU-6 (Fig. 1(a) and (b)) returned a mean particle size of 2.50 ± 0.57 nm, compared to 1.54 ± 0.32 nm from CO adsorption isotherms. These values are in general agreement if one takes in to account the error ranges quoted. Thus, with respect to Table 1 and Fig. 1, GU-6 represents a well dispersed Pd catalyst, with a mean Pd particle size of approximately 2.0 nm.

3.1.2. CO temperature-programmed IR

Fig. 2 presents the post CO saturation TP-IR DRIFTS spectra of GU-6 as a function of increasing desorption temperature. At 28 °C four spectral features are distinguishable: a shoulder feature at 2072 cm^{-1} and a peak at 2051 cm^{-1} corresponding to linear CO adsorption on corner and edges sites, respectively, and two broad features at 1964 and 1884 cm^{-1} assigned to adsorption of μ_2 bridge-bonded CO on Pd(100) planes and μ_3 bridge-bonded CO on Pd(111) planes, respectively [2,19]. Peak intensity was observed to decrease as desorption temperatures were systematically elevated. The following CO adsorption binding strength to GU-6 was established: μ_3 bridge-bonded CO on Pd(111) > μ_2 bridge-bonded CO on Pd(100) ≈ linear CO (edge) > linear CO (corner). Peak shifting for IR features associated with bridge-bonded CO adsorption were distinct; shifts from 1964 – 1945 cm^{-1} and 1886 – 1771 cm^{-1} were observed for μ_2 and μ_3 bridge-bonded CO, respectively. These shifts result from lateral interactions between neighbouring molecules due to dipole coupling effects, which reduce with decreasing surface coverage [20].

These designated wavenumber values and distinction of 2 linear CO adsorption sites for Pd/Al_2O_3 catalysts closely align with previous investigations [2–4,19]. However, the distribution of the μ_2 $CO_{(ads)}$ on Pd (100) and μ_3 $CO_{(ads)}$ on Pd(111) spectral features differ. Typically, peak height of the μ_2 bridge-bonded CO on Pd(100) feature (1964 cm^{-1}) is equal to, and more frequently greater than, that of the μ_3 $CO_{(ads)}$ on Pd (111) feature (1884 cm^{-1}). GU-6 presents the opposite trend. Fig. 3 contains the CO saturation coverage spectra for CO adsorption over Pd crystallites of GU-6 (black), GU-2 (red) and GU-4 (blue), where GU-2 [3] and GU-4 [4] represent previously investigated 0.3 wt% Pd/Al_2O_3 catalysts. Table S1 describes the specification for each of these Pd/Al_2O_3 catalysts. For clarification purposes, the spectrum presented as GU-4 was obtained from a 1 wt% Pd/Al_2O_3 catalyst which was then diluted to 0.3 wt% Pd loading with alumina; as such, the spectrum is representative of the Pd crystallites associated with the diluted 0.3 wt% Pd catalyst, GU-4. Reference to Fig. 3 highlights a clear discrepancy in the ratio

Table 1
Metal loading, surface area, uptake of CO, concentration of surface Pd atoms, dispersion, and particle size for GU-6. Catalyst dispersion and particle size values are calculated from CO uptake.

Pd Loading (AAS) (wt %)	BET (m^2 g^{-1})	Saturation coverage of CO (μmol CO g^{-1} $_{(cat)}$)	Surface Pd atoms (μmol $g^{-1}_{(cat)}$)	Catalyst Dispersion (%)	Calc. Mean Pd Particle size (nm)
0.38 ± 0.01	119.6 ± 3.59	10.0 ± 2.10	20.0 ± 4.11	70.8	1.54 ± 0.32

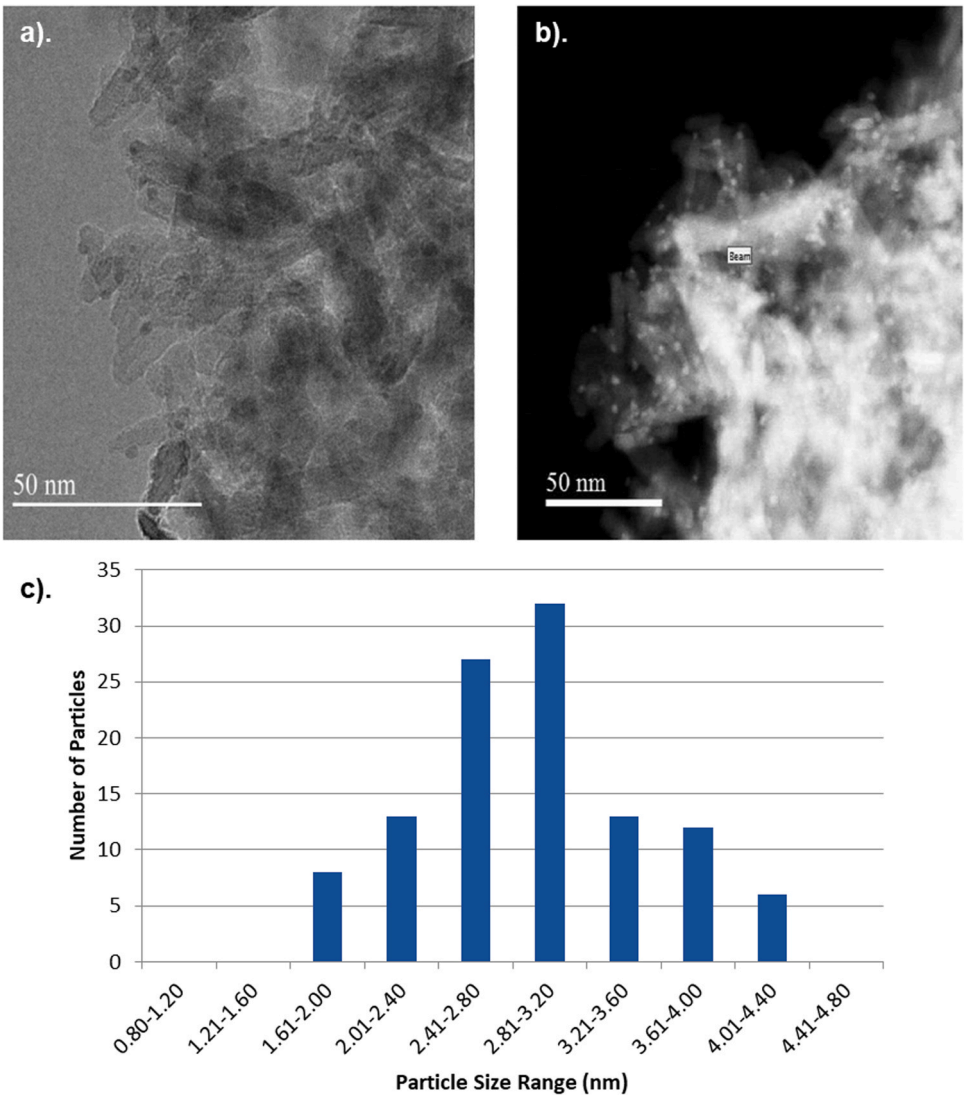

Fig. 1. TEM image micrographs of as received GU-6: a). bright field and b). high angle dark field. Dark spots (a) and light spots(b) are assigned as Pd particles. Scale bars = 50 nm. c). TEM derived particle size distribution of as-received GU-6.

of the Pd(100) *vs.* Pd(111) spectral features for GU-6 compared to that of GU-2 and GU-4, with the Pd(111) plane established as far more prevalent than the Pd(100) for GU-6. Thus, we propose that GU-6 possesses small Pd crystallites (*ca.* 2 nm) such that the Pd(100) plane (1964 cm^{-1}) is significantly minimised compared to the Pd(111) (1884 cm^{-1}). Nitrobenzene adsorption occurs over Pd(111) in a vertical orientation *via* one Pd-O bond – a parameter which minimises formation of nitrobenzene derived by-products through the perpendicular orientation of the benzene ring to the active Pd surface [5]. Therefore, the pre-dominant nature of the Pd(111) plane is expected to be beneficial to aniline formation over GU-6.

3.2. Reaction testing

3.2.1. Vapour phase

Fig. 4 displays nitrobenzene conversion (grey) and aniline selectivity (red) as a function of increasing reaction run time for vapour phase nitrobenzene hydrogenation with GU-6 at 160 °C over a 120 h period. Both reagent conversion and product selectivity varied with time on stream, exhibiting opposing trends. Initially, nitrobenzene conversion reached ≥ 99.98% until 25 h on stream, after which conversion systematically declined with increasing time on stream and seemingly asymptotes to a value of *ca.* 26% after 105 h. The observed decline in nitrobenzene conversion during reaction testing differed from previous investigations by the authors, in which two 0.3 wt% Pd/Al_2O_3 catalysts maintained conversion throughout reaction testing [3,4]. In contrast, aniline selectivity was maximised with reaction run time, increasing from an initial value of 93% and reaching ≥ 99% from 20 h onwards. A parametric investigation of liquid phase nitrobenzene hydrogenation utilising a 0.3 wt% Pd/Al_2O_3 catalyst in a fixed bed tubular reactor by Sá Couto et al. noted an increase in product selectivity with reaction duration, yet in this instance nitrobenzene conversion remained near complete throughout and a product selectivity of > 99% was not achieved until 100 h T-o-S [10].

There is a direct coincidence between aniline yield and nitrobenzene conversion, as depicted in Fig. 5. Resultingly, aniline yield decreases from *ca.* 95 to 26% as the reaction progressed. Additionally, comparison of aniline selectivity alongside nitrobenzene conversion as a function of reaction time indicated that reagent conversion is not an impacting factor when considering the initial aniline selectivity increase – after 5 h run time aniline selectivity increased from *ca* 93 to 98% with no change in nitrobenzene conversion. Trends in reagent conversion and product selectivity with time on stream here indicate a catalyst conditioning phase is present; the authors propose nitrobenzene to be involved as a precursor for the steady-state surface operational phase of the catalyst.

Fig. 6 exhibits: a) aniline over-hydrogenation by-products

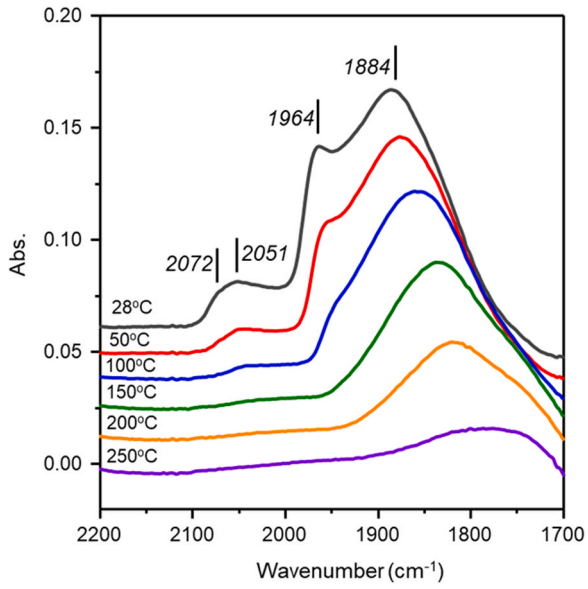

Fig. 2. CO temperature-programmed IR spectra for GU-6 as a function of increasing temperature. Spectra have been offset by 0.0125 a.u. to facilitate viewing.

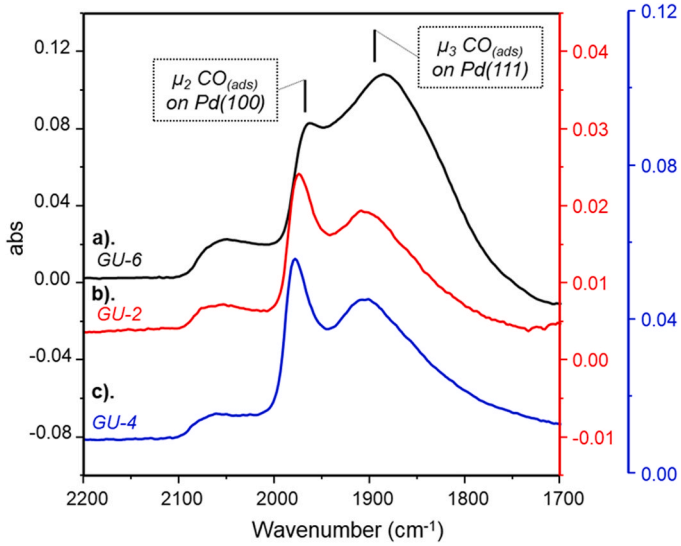

Fig. 3. CO TP-IR DRIFTS spectra of a saturation CO coverage over a) GU-6, b). GU-2 and c). GU-4. GU-2 and GU-4 saturation spectra are recreated from references [3,4], respectively. Note the 3 varying y-axes.

dicyclohexylamine (DICHA), N-cyclohexylaniline (CHAN) and cyclohexylamine (CHA) alongside benzene (BZ) and b) nitrobenzene derived intermediates cyclohexanol (CHOL), cyclohexanone (CHO), cyclohexanone oxime (CHOX) and phenol (PHOL) as a function of reaction run time. Initial aniline derived by-product selectivity values were as follows: DICHA = 2.5%, CHAN = 0.4% and CHA = 1.8%. This distribution of selectivity agrees with previous data sets at elevated hydrogen loading in which DICHA % > CHA % > CHAN % [3,4]. DICHA, CHA and BZ exhibited varied reaction trends in comparison to CHAN. The former set of products decreased with time on stream, such that after 10 h the Pathway 1 aniline over-hydrogenation by-products DICHA and CHA were no longer observable. Diversly, CHAN selectivity was observed to increase at 20 h, after which selectivity decreased with observation of CHAN extremely limited after 40 h and no longer an observable by-product after 70 h reaction time. Thus, 40 h after reaction with GU-6

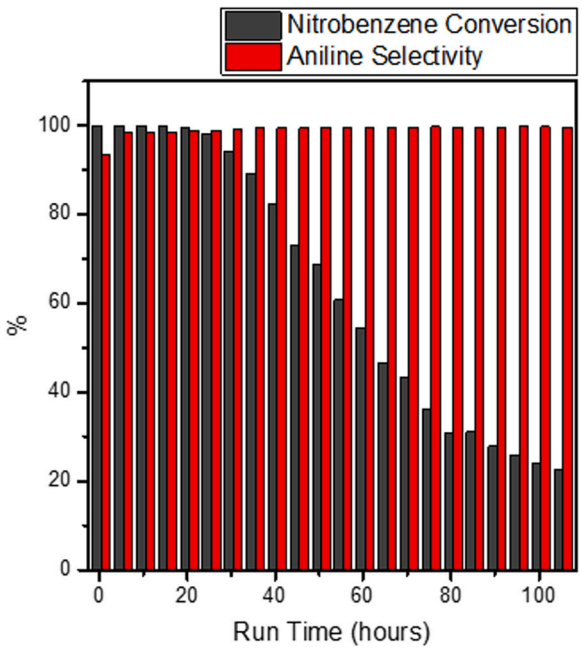

Fig. 4. Vapour phase nitrobenzene conversion (grey columns) and aniline selectivity (red columns) as a function of time on stream. Reaction temperature: 160 °C. Incident flux: 1.44 $\mu mol_{(NB)}$ min^{-1}. H_2:$C_6H_5NO_2$ molar flow ratio = 600:1. WHSV = 0.33 h^{-1}.

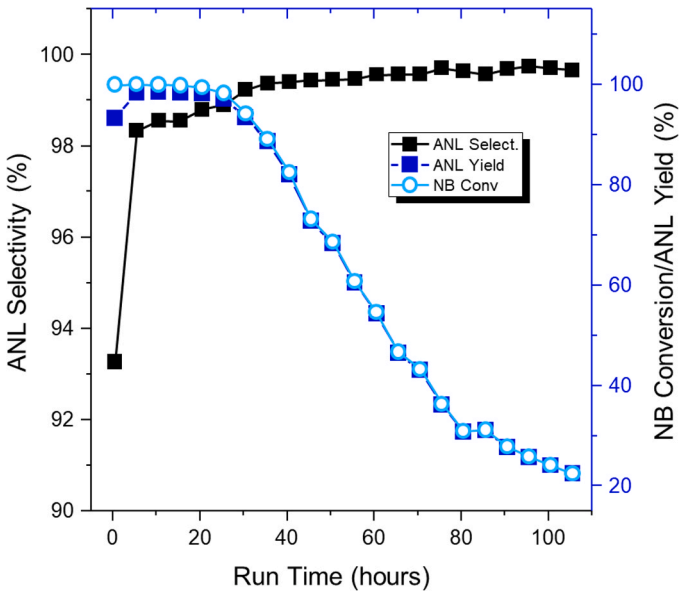

Fig. 5. Plot depicting nitrobenzene conversion (light blue circle points), aniline selectivity (black square points) and aniline yield (dark blue square points) as a function of time on stream. Note the differing y-axes. Reaction temperature: 160 °C. Incident flux: 1.44 $\mu mol_{(NB)}$ min^{-1}. H_2:$C_6H_5NO_2$ molar flow ratio = 600:1. WHSV = 0.33 h^{-1}.

at 160 °C resulted in a significantly minor contribution to catalytic outputs from Pathway 1 by-products, with this pathway eliminated completely after 70 h′ time on stream.

Nitrobenzene derived by-products exhibit varied selectivity trends. All three Pathway 2 by-products (CHOL, CHO and CHOX) are observable at some point in the reaction coordinate (Fig. 6(b)). CHOL is observed with *ca.* 0.3% selectivity initially and is no longer observable by the next sampling point, CHO selectivity varies between 0.05 – 0.15% throughout the run time with no trend observed and CHOX emerged

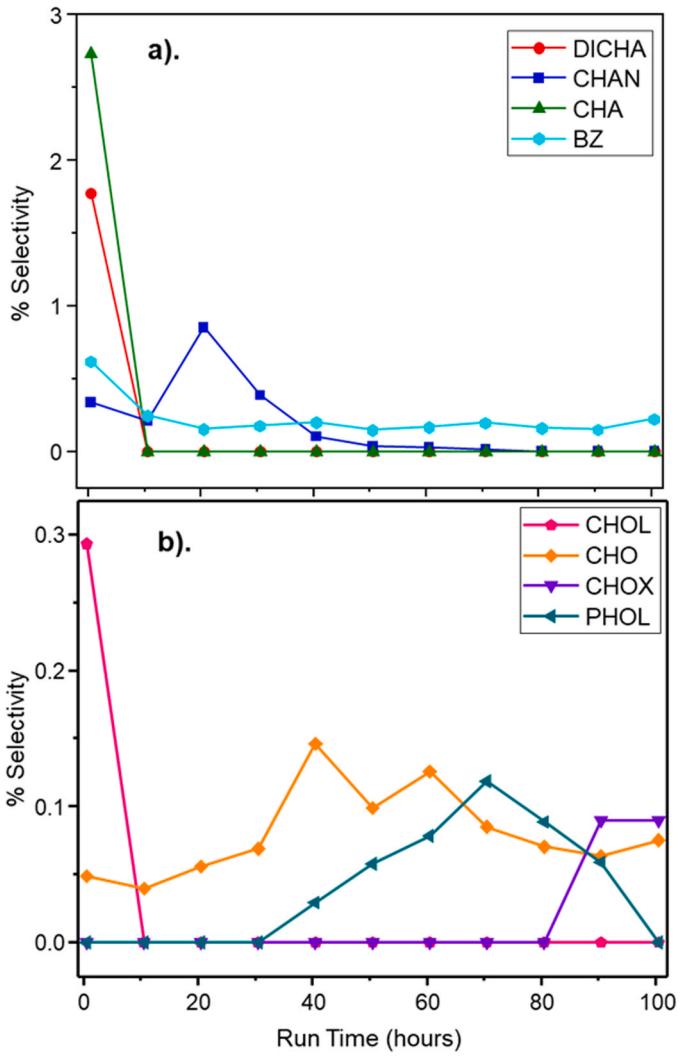

Fig. 6. Vapour phase selectivity values of a). BZ (light blue) and aniline over-hydrogenation by-products CHA (green), CHAN (blue) and DICHA (red) and b). PHOL (light green) and nitrobenzene derived intermediates CHOX (purple), CHO (orange) and CHOL (pink). Reaction temperature: 160 °C. Incident flux: 1.44 $\mu mol_{(NB)}$ min^{-1}. H_2:$C_6H_5NO_2$ molar flow ratio = 600:1. WHSV = 0.33 h^{-1}.

after 90 h′ time on stream at *ca.* 0.1%. The decline in CHOL selectivity over the initial 10 h′ time on stream reflects the decreased hydrogenation ability of GU-6 as catalyst conditioning progressed. PHOL production (Pathway 4 by-product) is observed between a run time of 40 - 100 h.

Overall, vapour phase nitrobenzene hydrogenation at a temperature of 160 °C over GU-6 presented high aniline selectivity, a loss of nitrobenzene conversion, and Pathway 1 by-products (DICHA, CHA and CHAN) to be the dominant route to lowered aniline selectivity. However, importantly, this pathway was limited after 40 h run time and completely shut down after 70 h T-o-S. For reference, blank reaction testing on a reference γ-alumina sample performed by Morisse and co-workers revealed minimal nitrobenzene conversion [3], therefore it is deduced that all the hydrogenation activity is attributed to the presence of the Pd nanoparticles. However, a subsequent infrared investigation of nitrobenzene adsorption over a 5 wt% Pd/γ-Al_2O_3 catalyst by McCullagh and co-workers revealed that the product, aniline, adsorbs on the support material, where it undergoes no further transformation and eventually desorbs [5].

3.2.2. *Liquid phase*

Fig. 7 presents nitrobenzene conversion and aniline selectivity for a) liquid and b) vapour phase nitrobenzene hydrogenation over GU-6. The vapour phase data set is the same as discussed in Section 3.2.1., however it is presented over a 25-hour run time, so that it may be compared to the time-constrained liquid phase dataset. Liquid phase nitrobenzene hydrogenation over GU-6 demonstrated complete nitrobenzene conversion throughout the duration of reaction testing (Fig. 7(a)). Additionally, a small increase in aniline selectivity was observed from 99.2% at the initial sampling point to ≥ 99.9% after 8 h run time. This initial liquid phase aniline selectivity is far higher than the 20% reported by Sá Couto et al. obtained with a comparable 0.3 wt% Pd/Al_2O_3 commercial catalyst after a run time of *ca.* 28 h [10]. In fact, aniline selectivity of > 99% was not achieved until *ca.* 100 h run time, reflecting the exceptional liquid phase aniline selectivity achieved rapidly with industrial prototype catalyst GU-6.

Due to the complete conversion of nitrobenzene during liquid phase reaction testing herewith, aniline yield (Fig. 8) is governed by aniline selectivity, exhibiting a maximum of 99.9% for elevated temperature. As observed with vapour phase testing, the initial increase in product selectivity, from 99.2 to 99.8%, observed for liquid phase testing is

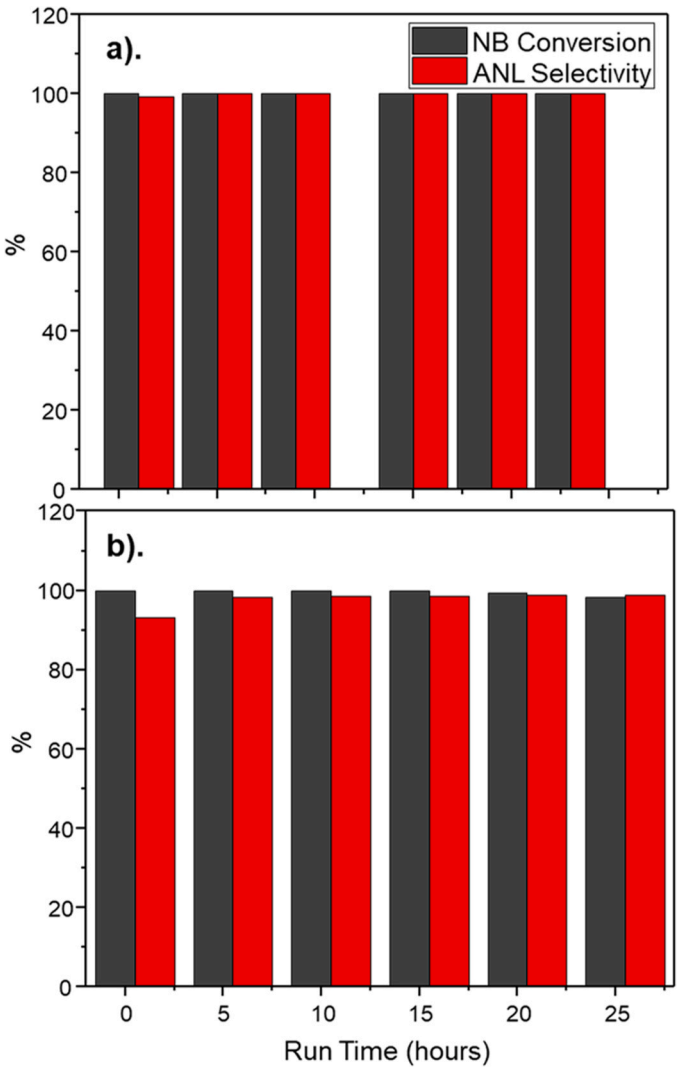

Fig. 7. Nitrobenzene conversion (grey) and aniline selectivity (red) over 25 h for a) liquid and b) vapour phase nitrobenzene hydrogenation over GU-6. Reaction conditions: [a - temperature: 160 °C. Incident flux: 1.44 $\mu mol_{(NB)}$ min^{-1}. H_2:$C_6H_5NO_2$ molar flow ratio = 600:1. WHSV = 0.33 h^{-1}]; [b - temperature: 265 °C. Incident flux: 14% w/w nitrobenzene in aniline. Pressure: 20 barg].

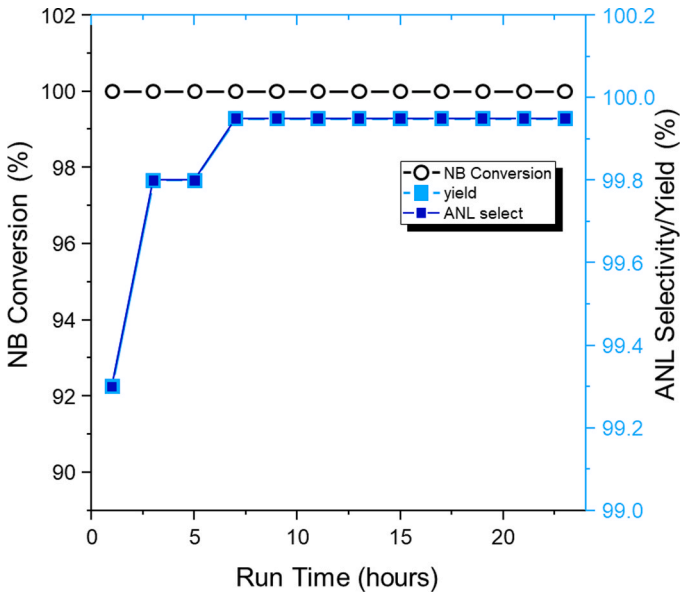

Fig. 8. Plot depicting liquid phase nitrobenzene conversion (black circle points), aniline selectivity (dark blue square points) and aniline yield (light blue square points) as a function of time on stream. Note the differing y-axes. Reaction temperature: 265 °C. Incident flux: 14% w/w nitrobenzene in aniline. Pressure: 20 barg.

independent from any variance in reagent conversion. A second increase in aniline selectivity is observed from 99.8 to 99.9% after 7 h run time.

Pathway 1 by-products (Fig. 9(a)), arising from the over-hydrogenation of aniline, are reduced for liquid phase testing *vs.* vapour phase (Fig. 6(a)); the maximum by-product selectivity observed for the liquid phase was CHAN at 0.46% *vs.* 2.70% for DICHA in the vapour phase. However, when considering the overall impact of prolonged run time on pathway 1 by-product selectivity the same trend is apparent for both phases: formation of aniline derived by-products declined with increasing time on stream for liquid and vapor phase nitrobenzene hydrogenation with GU-6. When excluding the initial sample point for vapour phase testing, which yielded elevated levels of DICHA and CHA owed to the absence of any catalyst conditioning, both data sets show the coupling product CHAN to be the dominant by-product. In the liquid phase, CHAN steadily decreases with time on stream and plateaus at *ca.* 0.02% after 7 h run time. No DICHA was observed during liquid phase reaction testing. This outcome is thought to reflect mass transfer induced hydrogen supply issues which are not experienced during the vapour phase reaction testing. Additionally, the authors recognise the higher turnover associated with chemistry in the liquid phase and appreciate that this renders the data sets not directly comparable. Nevertheless, the clear similarity in degradation of pathway 1 by-products for both phases with prolonged nitrobenzene hydrogenation (Figs. 6 and 9) merits acknowledgement and indicates that outcomes established from characterisation post-vapour phase analysis could be reasonably applied to rationalise liquid phase outcomes.

Fig. 9(b) presents a collection of minor by-products (BZ, CHO, CHOL and PHOL) observed during liquid phase testing which amount to a maximum selectivity of $< 0.2\%$. These by-products decline with time on stream with selectivity values stabilised after 7 h run time, the same time exhibited for the stabilisation of CHAN selectivity. After this time point BZ is no longer detected, CHOL selectivity is $< 0.01\%$ and CHO and PHOL both present values of *ca.* 0.02%. These results vary compared to vapour phase testing, in which production of CHO and PHOL did not present distinct trends. However, to re-iterate, vapour phase and liquid phase testing results suggest coincidence between trends experienced for Pathway 1 by-products – the main route to reduced aniline yields [3,4].

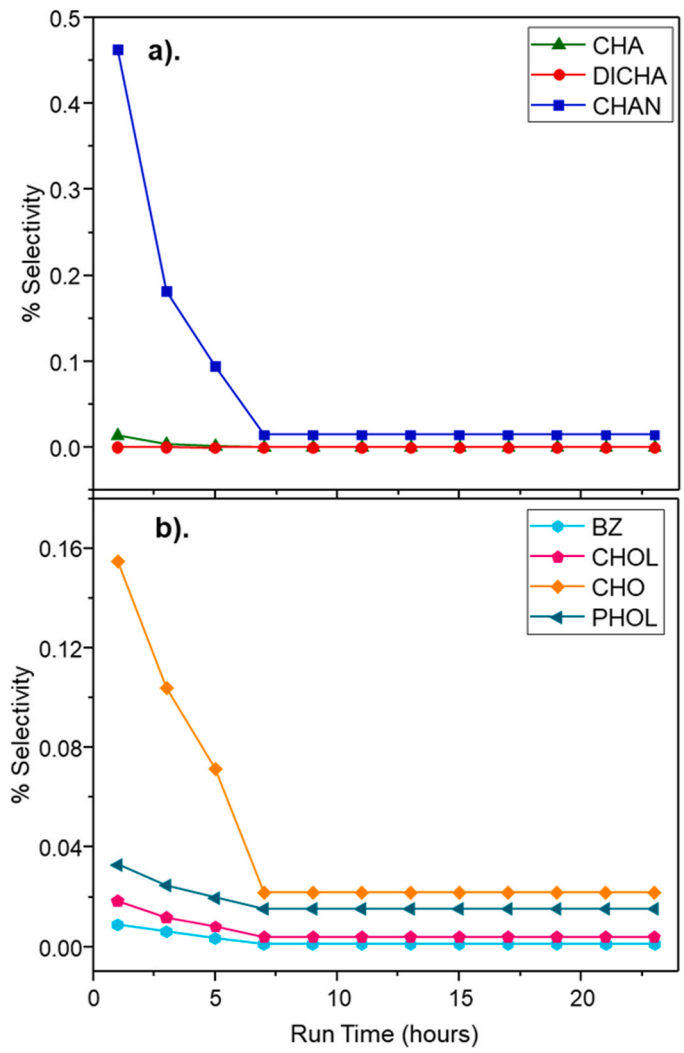

Fig. 9. Liquid phase selectivity values for a). aniline over-hydrogenation by-products CHA (pink), CHAN (blue) and CHOL (pink) and b). BZ (light blue), PHOL (light green) and nitrobenzene derived intermediates CHO (orange) and CHOL (pink). Reaction temperature: 265 °C. Incident flux: 14% w/w nitrobenzene in aniline. Pressure: 20 barg.

The trend of improved aniline selectivity as a function of T-o-S as observed in this section reproduces outcomes reported by Sá Couto and co-workers in their examination of liquid phase nitrobenzene hydrogenation in a tubular fixed-bed reactor using a low loading Pd/Al_2O_3 catalyst [10]. Ideally, it would have been desirable to explore the liquid phase studies over the 120 h duration undertaken for the vapour phase studies but that was not possible (see Section 2.2.2). It is anticipated that the dramatic loss of activity observed in the vapour phase over the period 40–100 h (Figs. 4 and 5) will be lessened in the liquid phase due to the moderating presence of solvent molecules. More work, beyond the scope of this article, is required to explore this matter further.

3.3. Catalyst characterisation: post-reaction

All post-reaction characterisation is obtained after vapour phase nitrobenzene hydrogenation with GU-6 (Conditions: temperature = 160 °C; H_2:$C_6H_5NO_2$ molar flow ratio = 600:1; WHSV = 0.33 h^{-1}).

3.3.1. BET and TEM

Post-reaction, BET derived surface area was 123 ± 1.20 m^2 g^{-1}. Comparison with the pre-reaction value, 119.6 ± 3.59 m^2 g^{-1}, indicated the effective retainment of catalyst surface area during nitrobenzene

hydrogenation at elevated temperature with GU-6. Fig. 10 presents post-reaction GU-6 bright field (a) and dark field (b) TEM micrograph images. An average particle size of 2.45 ± 0.60 nm was deduced, within error matching the as received sample and thereby signifying the absence of any sintering mechanism during reaction testing.

3.4. Temperature-programmed oxidation

Temperature-programmed oxidation (TPO) measurements for GU-6 as a function of time on stream for nitrobenzene hydrogenation are presented in Fig. 11. After 1 h a sharp desorption feature arising from a nominally named α carbon species was recorded at 275 °C. As time on stream progressed a second carbon feature, β, emerged with a desorption maximum temperature of 328 °C. A third carbon species, named γ, was distinct after 21.5 h run time at a temperature maximum of 484 °C, representing a more strongly bound carbon on the catalyst surface. The intensity of peaks for the β and γ carbon species increased with time on stream.

Fig. 12 presents a comparison of nitrobenzene conversion *vs.* the total peak area for all TPO derived carbon features deposited on GU-6 (Fig. 11) as a function of time on stream. A clear interrelationship between reagent conversion and formation of carbon residues on GU-6 is

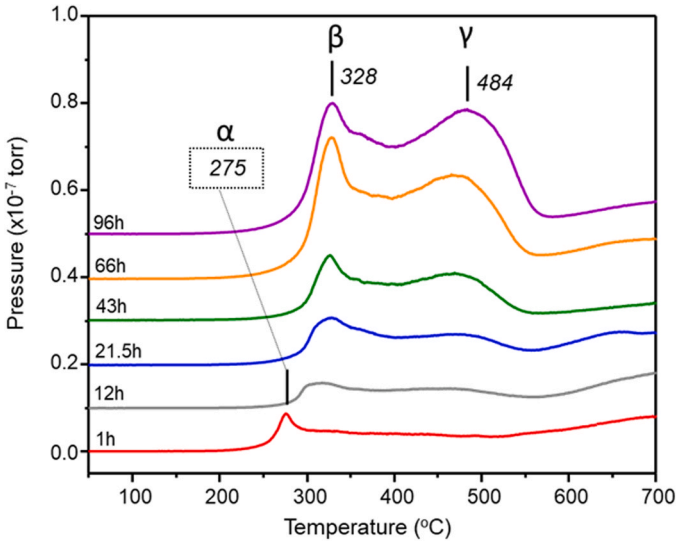

Fig. 11. Temperature-programmed oxidation measurement of GU-6 post-reaction as a function of increasing time on stream.

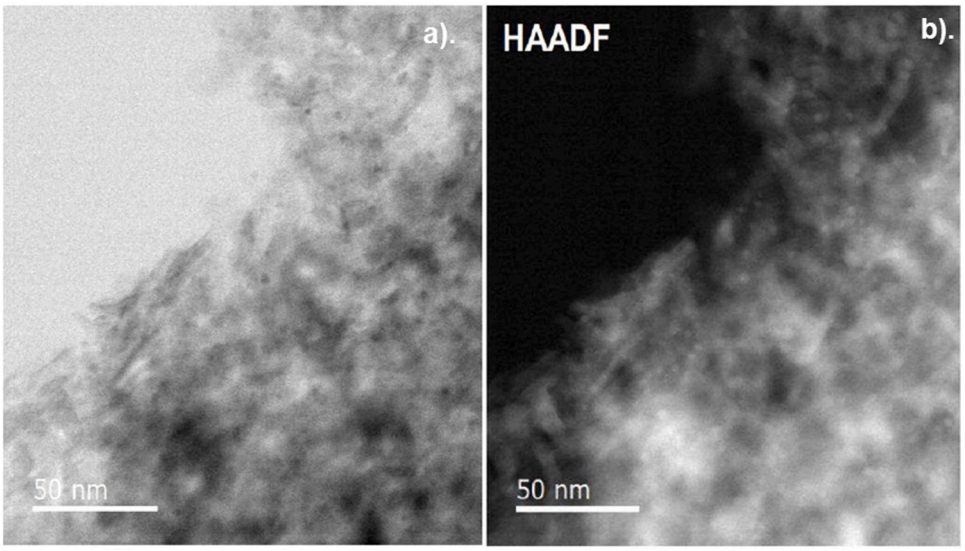

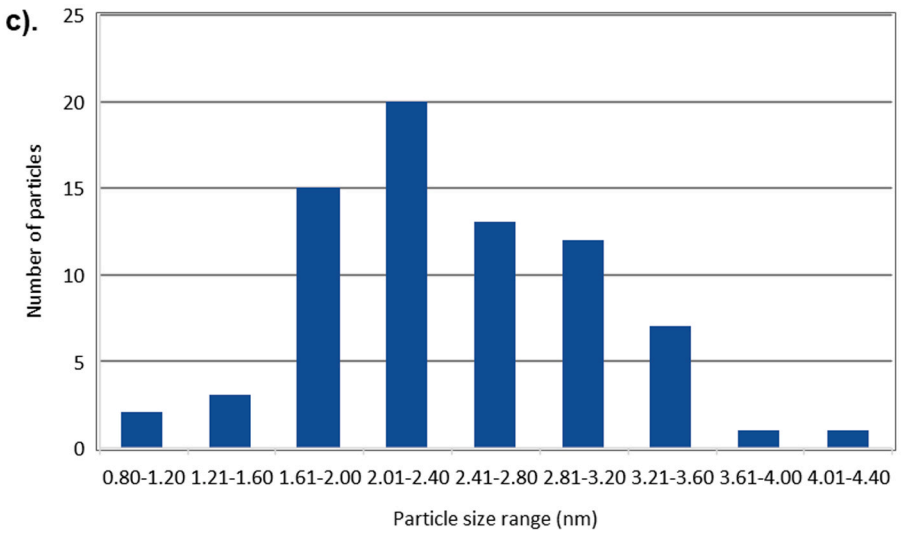

Fig. 10. TEM image micrographs of GU-6 post nitrobenzene hydrogenation: a). bright field and b). high angle dark field. Dark and light spots are assigned as Pd particles, respectively. Scale bars = 50 nm. c). TEM derived particle size distribution of GU-6 post-reaction.

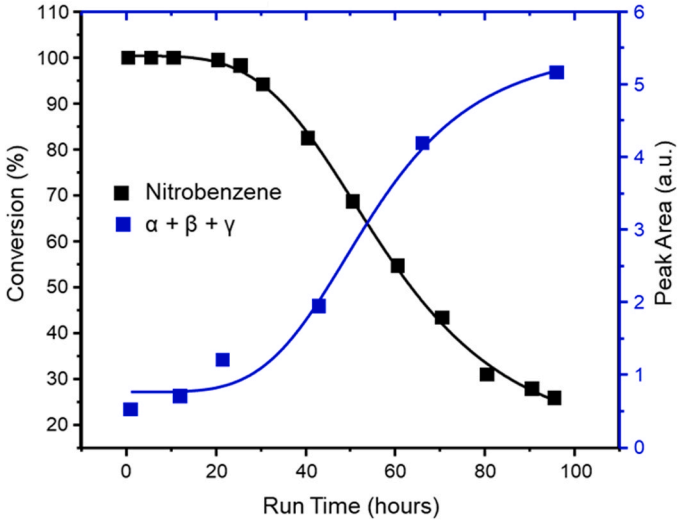

Fig. 12. Comparison of nitrobenzene conversion and TPO total carbon peak area over GU-6 as a function of time on stream.

presented. As deposition of carbon on the catalyst surface increased, nitrobenzene conversion showed a concomitant decrease. Thus, a deactivation mechanism *via* coking is identified during nitrobenzene hydrogenation over GU-6.

3.5. Catalyst regeneration

Post-reaction regeneration of GU-6 was examined to assess whether nitrobenzene conversion activity could be restored without re-opening aniline over-hydrogenation chemistry. Vapour phase nitrobenzene hydrogenation with the re-reduced catalyst is presented in the Supporting Information section (Figs. S4 and S5) over an 18-hour time-period. Fig. S4 presents nitrobenzene conversion and aniline selectivity as a function of T-o-S and establishes the return of complete reagent conversion for the initial sampling point. Interestingly, a higher initial aniline selectivity is associated with the re-reduced catalyst: 97% compared to 93% for the fresh catalyst. Thus, after the regeneration process GU-6 remained highly selective for aniline production. However, this 97% aniline selectivity post re-reduction is reduced compared to the 99.8% selectivity achieved with extended run time during the first round of reaction testing (Figs. 4 and 5). Reference to Fig. S5a demonstrates the re-emergence of pathway 1 by-products CHA, CHAN and DICHA. Therefore, although reduction of GU-6 at a lowered temperature did permit recovery of nitrobenzene conversion, it did so at the expense of re-introducing by-products to the product stream.

4. Discussion

Concepts from reaction testing and catalyst characterisation will be combined at this juncture to present the dominant origin of aniline by-product formation with industrial prototype catalyst GU-6, which is governed by a specific crystallite morphology. Vapour phase nitrobenzene hydrogenation with GU-6 at 160 °C displayed opposing trends for nitrobenzene conversion and aniline selectivity. This outcome mimics trends reported by Sá Couto and co-workers in their examination of liquid phase nitrobenzene hydrogenation in a tubular fixed-bed reactor using a low loading Pd/Al_2O_3 catalyst [10]. For our vapour phase studies, reagent conversion decreased from 20 h′ time on stream from *ca.* 99.9 to 26.4% after 105 h, while aniline selectivity increased. Improved product selectivity followed a decline in, and complete shut down after 70 h, of aniline over hydrogenation by-products CHA, CHAN and DICHA. This is associated with the advancement of a catalyst conditioning phase. We propose that initially high nitrobenzene conversions reflect an element of reagent transformation to a hydrocarbonaceous residue deposited on the catalyst surface which enhances product selectivity [21]. Thus, aniline selectivity is maximised with GU-6 at 160 °C after 70 h run time and is owed to the shutdown of production of Pathway 1 by-products during a catalyst conditioning phase.

GU-6 outperforms a previously investigated 0.3 wt% Pd/Al_2O_3 catalyst, GU-2 [3], for nitrobenzene hydrogenation at elevated temperatures; a parameter of importance for industry to permit energy recovery processes on plant *via* the generation and utilisation of superheated steam [17]. GU-2 exhibited an aniline selectivity of 75.2% at 160 °C with a H_2 : NB ratio of 600:1 and a *ca.* 21-hour catalyst conditioning period [3]. Here, GU-6 yields a product selectivity of 98.7% after the same conditioning period and reaction conditions. Clearly, GU-6 is a significantly more selective aniline synthesis catalyst. An additional 0.3 wt% Pd/Al_2O_3 catalyst, GU-4 [4], was examined after a *ca.* 52-hour conditioning phase under a lowered H_2 : NB ratio (40:1) and temperature (140 °C). Again, GU-6 presented the greater aniline selectivity (99.6 *vs.* 96.7%). This observation highlights the superiority of industrial prototype catalyst GU-6 as a candidate for nitrobenzene hydrogenation compared to previously investigated 0.3 wt% Pd/Al_2O_3 catalysts for vapour phase testing. Comparison of saturation coverage CO IR spectra of GU-2, GU-4 and GU-6 (Fig. 3) revealed industrial prototype catalyst GU-6 possessed a minimised number of Pd(100) adsorption sites compared to GU-2 and GU-4. Thus, it is tentatively proposed that this minimisation of the Pd(100) facet exhibited by GU-6 is responsible for the improved product selectivity observed.

Fig. 13 presents the room temperature CO saturation IR DRIFTS spectra of a). unreacted GU-6 and b). post-reaction GU-6. Here, reaction testing was performed with GU-6 in pellet form to facilitate collection of adequate IR spectra *via* the "scraping" technique detailed in the experimental section. A reaction temperature of 160 °C and a H_2 : NB ratio of *ca.* 600:1 was utilised, as with the powdered GU-6 reaction testing detailed in Section 3.2.1. Comparable selectivity trends were observed for GU-6 in powder and pelleted form for these conditions.

Fig. 13 shows stark differences in CO IR spectra collected pre- and post-nitrobenzene hydrogenation with GU-6. Namely, the significant reduction in the IR feature associated with μ_2 $CO_{(ads)}$ on Pd(100), observed as a distinguished feature at 1964 cm^{-1} in the fresh sample and a small shoulder feature in the post-reaction sample, an indication that the Pd(100) facet has been significantly compromised during reaction testing. Additionally, two broad IR features are distinct post-reaction at

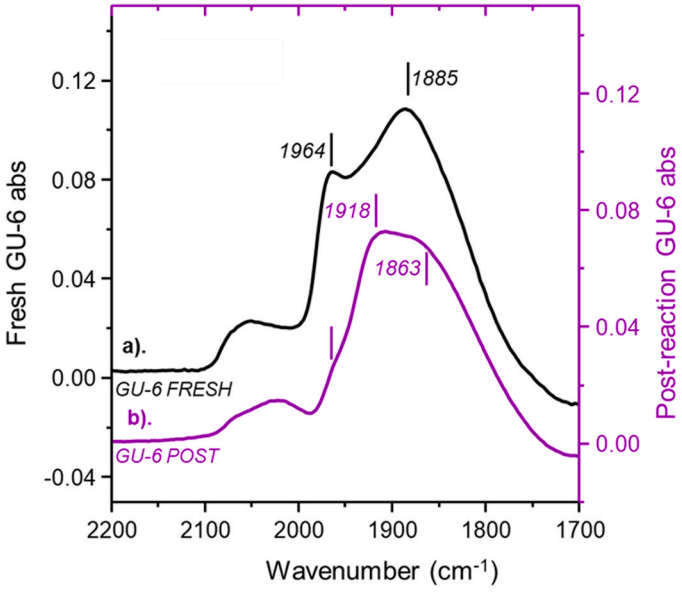

Fig. 13. Room temperature saturation coverage CO IR DRIFTS spectra of a). fresh and b). post-reaction GU-6. Note the differing y-axes.

1918 and 1863 cm^{-1}. The later wavenumber value is a typical frequency associated with μ_3 bridge-bonded $CO_{(ads)}$ on Pd(111) as CO coverage is decreased [2–4,19]. As previously introduced, the IR feature associated with μ_2 $CO_{(ads)}$ on the Pd(100) also experiences a descent in wavenumber value with decreasing surface area; however, a separate CO IR measurement of GU-6 as a function of run time (Supporting Information, Fig. S3) showed both the IR feature at 1918 cm^{-1} alongside the band at 1964 cm^{-1}, associated with μ_2 $CO_{(ads)}$ on the Pd(100), after 16 h run time. Therefore, the feature at 1918 cm^{-1} post-reaction is not associated with shifted μ_2 $CO_{(ads)}$ on Pd(100). An investigation by Tüshaus et al. into CO adlayers on Pd(111) utilising infrared reflection-absorption spectroscopy (IRAS) and LEED identified an IR feature at 1920 cm^{-1} as originating from μ_2 bridge-bonded $CO_{(ads)}$ on Pd(111) [22]. Thus, emergence of an IR feature at 1918 cm^{-1} is assigned to an element of μ_2 $CO_{(ads)}$ on the Pd(111) facets of GU-6.

The significant reduction in the 1964 cm^{-1} feature associated with CO adsorption to Pd(100) and of lower co-ordinated CO (2-fold) on the Pd(111) facet post-reaction (Fig. 13b) indicates predominant and partial blocking of the respective adsorption sites. TPO measurements revealed increasing degrees of carbon laydown with time on stream (Fig. 11), with the reagent, nitrobenzene, purported to act as a carbon precursor. Therefore, we propose that during nitrobenzene hydrogenation at elevated temperature with GU-6 the Pd(100) facet is largely compromised *via* predominant blocking of adsorption sites from carbon laydown, with some carbon laydown also impacting, but not entirely impeding, adsorption to the Pd(111) planes. Consideration of the morphological detail obtained here, and reaction testing outcomes, now permits confirmation of an above-introduced hypothesis – namely, the minimised Pd(100) facet of GU-6 is the origin of its superior aniline selectivity compared to GU-2 and GU-4. After a conditioning phase, we assert the absence of pathway-1 by-products (Fig. 6) and the significant compromisation of Pd(100) facets (Fig. 13). Therefore, it follows that the predominant blocking of adsorption sites on Pd(100) with T-o-S has prevented the over-hydrogenation of aniline. Reflecting on this hypothesis, thus indicates that the Pd(100) plane is responsible for product over-hydrogenation, the dominant route to lowered aniline selectivity during nitrobenzene hydrogenation [3,4].

Fig. 14 presents a graphical representation of the Pd crystallites of GU-6 a). pre-reaction and b). post-reaction, for an extended time. Prior to conditioning, all sites of the catalyst are accessible; thus, nitrobenzene conversion is complete and aniline over-hydrogenation is possible. Initially Pd(100) facets are fully available for aniline adsorption, yet aniline selectivity was still high (93%) at this stage. This is owed to the large Pd(111) planes and small Pd(100) planes associated with GU-6. Additionally, nitrobenzene adsorption has been determined to occur vertically over the Pd(111) plane *via* a single oxygen-metal interaction from DRIFTS measurements [5]. This adsorption configuration acts to keep the aromatic moiety of nitrobenzene perpendicular from the active Pd surface, inhibiting formation of nitrobenzene derived by-products. As the reaction progresses (Fig. 14 b)), carbon laydown results and leads to the predominant blocking of Pd(100) adsorption sites. This prevents aniline re-adsorption to the Pd crystallites of GU-6, thereby preventing formation of pathway-1 by-products and improving aniline selectivity, as highlighted in reaction testing data (Figs. 4 - 6). Carbon is also deposited on Pd(111). This does not entirely stop nitrobenzene adsorption, but it does limit it, as reflected in the observed decrease of nitrobenzene conversion as the reaction progressed (Fig. 5). Overall, aniline selectivity is thus maximised for alumina supported Pd catalysts in the possession of predominantly Pd(111) planes and minimised Pd (100) facets. This observation thereby becomes a critical parameter for the design of optimised Pd catalysts for high aniline selectivity catalysis at elevated temperature.

By-products arising from a direct transformation of nitrobenzene, Pathway-2 (CHO, CHOL and CHOX) and Pathway-4 (PHOL), exhibited no decline in selectivity with the loss of the Pd(100) plane, but were instead minimal contributors throughout reaction testing. This indicates

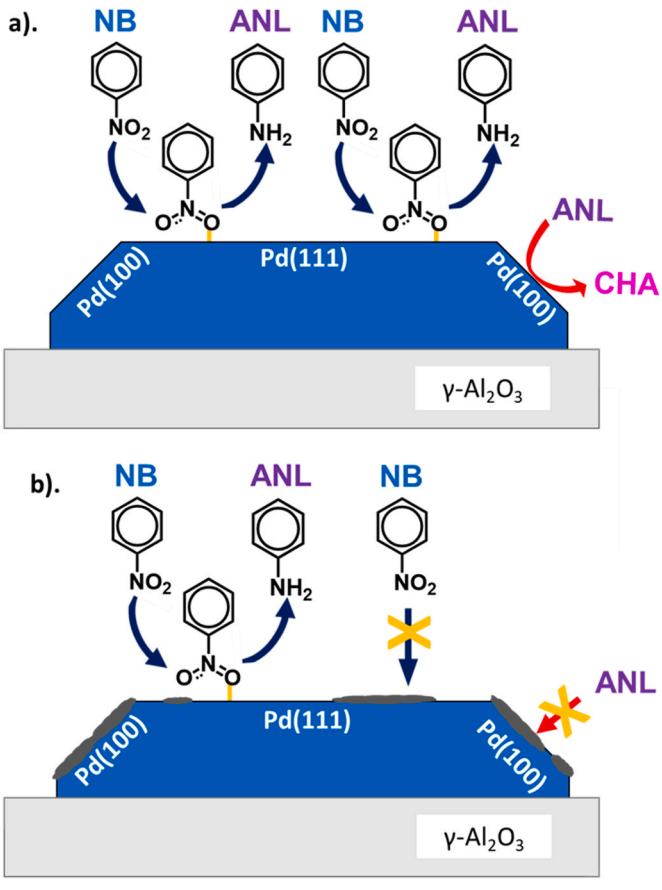

Fig. 14. Graphic depicting Pd(100) and Pd(111) planes of Pd crystallites of GU-6 a). pre- and b). post-nitrobenzene hydrogenation at 160 °C for an extended run time. Dark grey sites represent areas of C laydown.

that transformation of nitrobenzene to such products arises on the Pd (111) plane, the same plane as nitrobenzene hydrogenation through to aniline, or on defect sites within the Pd(111) plane. As such, prohibition of these by-products is not possible on GU-6. However, with an understanding of by-product distributions established, purification procedures (*e.g.*, distillation columns) can be implemented on plant which will be able to remove the trace levels of these by-products.

The restricted comparison of vapour and liquid phase reaction testing with GU-6 revealed similarities in aniline selectivity trends. That is, there was an increase in aniline selectivity with run time because of lowered over-hydrogenation of aniline. No definitive statements regarding morphological changes of GU-6 during reaction testing in the liquid phase can be made from vapour phase post-reaction characterisation herewith. However, the coincidence in aniline selectivity trends (Fig. 7) does suggest that aniline adsorption to the Pd(100) facet is also compromised with time on stream during liquid phase reaction testing.

5. Conclusions

Nitrobenzene hydrogenation with industrial prototype catalyst GU-6 at elevated temperature combined with CO IR and TPO measurements permitted identification of a specific Pd facet which governs aniline over-hydrogenation chemistry. The following conclusions can be drawn.

- Nitrobenzene conversion decreased and aniline selectivity increased as a function of run time for extended nitrobenzene hydrogenation in the vapour phase.

- Lab-scale vapour phase nitrobenzene hydrogenation with GU-6 at 160 °C showed fair comparison to liquid phase testing at 265 °C, parameters more akin to evolving industrial requirements.
- Catalyst characterisation revealed GU-6 to possess small Pd crystallites *ca.* 2 nm in size, and CO TP-IR measurements determined the Pd (111) planes to be dominant, with Pd(100) planes significantly less abundant than other 0.3 wt% Pd/Al_2O_3 technical grade catalysts tested.
- The Pd(100) plane is linked to aniline over-hydrogenation, and thus its minimisation is favourable.
- Pathways 2 and 4 by-products associated with nitrobenzene transformation are deemed to occur on Pd(111), the same site as nitrobenzene hydrogenation.
- The reaction chemistry described has been linked to a defined Pd crystallite morphology. This constitutes a heightened quality control parameter that may be relevant in defining catalyst specification requirements for application at the industrial complex.

CRediT author contribution statement

Campbell: Data curation, Investigation, Methodology. **McCullagh**: Data curation, Formal analysis, Investigation, Methodology, Validation, Visualization, Writing – original draft, Writing – review & editing. **McGrath:** Data curation, Investigation; **How**: Data curation, Investigation. **MacLaren**: Data curation, Investigation, Methodology. **Loenders**: Data curation, Investigation, Methodology; **Meyer**: Methodology, Supervision, Validation. **Carr**: Conceptualization, Funding acquisition, Investigation, Methodology; Project administration, Supervision, Validation. **Lennon**: Formal analysis, Investigation; Methodology, Project administration, Supervision, Validation, Writing – review & editing.

Declaration of Competing Interest

The authors declare the following financial interests/personal relationships which may be considered as potential competing interests. David Lennon reports financial support was provided by Huntsman International LLC Polyurethanes Division. David Lennon reports financial support was provided by Engineering and Physical Sciences Research Council. If there are other authors, they declare that they have no known competing financial interests or personal relationships that could have appeared to influence the work reported in this paper.

Data Availability

Data will be made available on request.

Acknowledgements

The EPSRC are thanked for the provision of Ph.D. studentships (JWC and ALMcC: EP/R513222/1; EP/N509668/1). Huntsman Polyurethanes are thanked for project support.

Appendix A. Supporting information

Supplementary data associated with this article can be found in the online version at doi:10.1016/j.apcata.2023.119541.

References

[1] G. Brereton, Polyurethanes, in: C. Ley, B. Elvers (Eds.), *Ullmann's Encyclopedia of Industrial Chemistry*, Wiley, Weinheim, 2019, pp. 1–76.
[2] A. McCullagh, R. Warringham, C. Morisse, L. Gilpin, C. Brennan, C. Mitchell, D. Lennon, Top. Catal. 64 (2021) 1010–1020.
[3] C. Morisse, A. McCullagh, J. Campbell, C. How, D. MacLaren, R. Carr, C. Mitchell, D. Lennon, Ind. Eng. Chem. Res. 60 (2021) 17917–17927.
[4] C. Morisse, A. McCullagh, J. Campbell, C. Mitchell, R. Carr, D. Lennon, Ind. Eng. Chem. Res. 61 (2022) 10712–10722.
[5] A. McCullagh, E. Gibson, S. Parker, K. Refson, D. Lennon, Phys. Chem. Chem. Phys. 25 (2023) 25993–26005.
[6] A. Corma, P. Concepción, P. Serna, Agnew. Chem. Int. Ed. 46 (2007) 7266–7269.
[7] S. Mukherjee, F. Libisch, N. Large, O. Neumann, L. Brown, J. Cheng, J. Lassiter, E. Carter, P. Nordlander, N. Halas, Nano Lett. 13 (2013) 240–247.
[8] Q. Zhang, J. Bu, J. Wang, C. Sun, D. Zhao, G. Sheng, X. Xie, M. Sun, L. Yu, ACS Catal. 10 (2020) 10350–10363.
[9] Z. Wang, Z. Yuan, R. Nie, Z. Hou, X. Zheng, Ind. Eng. Chem. Res. 49 (2010) 4664–4669.
[10] C. Couto, L. Madeira, C. Nunes, P. Araujo, Ind. Eng. Chem. Res. 56 (2017) 3231–3243.
[11] F. Haber, *Z. Electrochem*. Angew. Phys. Chem. 4 (1898) 506.
[12] E. Gelder, S. Jackson, C. Lok, Chem. Comm. (4) (2005) 522–524.
[13] K. Weissermal, H.J. Arpe, Industrial Organic Chemistry, Fourth Completely Revised Edition, Wiley-VCH, Heppenheim, Germany, 2003.
[14] A. Iluliianelli, T. Longo, A. Basile, J. Membr. Sci. 323 (2008) 235–240.
[15] Z. Wan, G. Li, C. Wang, H. Yang, D. Zhang, Catal 314 (2018) 107–113.
[16] Q.K. Tran, S. Han, H.V. Ly, S. Kim, J. Kim, J. Ind. Eng. Chem. 92 (2020) 243–251.
[17] C. Mitchell, D. Stewart, WO2011113491 - Process for the conversion of aromatic nitro compound into amines, Huntsman International LLC, Utah, 2011.
[18] T. Lear, R. Marshall, E. Gibson, T. Schütt, T. Klapötke, G. Rupprechter, H. Freund, J. Winfield, D. Lennon, Phys. Chem. Chem. Phys. 7 (2005) 565.
[19] T. Lear, R. Marshall, J. Lopez-Sanchez, S. Jackson, T. Klapotke, M. Baumer, G. Rupprechter, H. Freund, D. Lennon, J. Chem. Phys. 123 (2005), 174706.
[20] P. Hollins, Spectro Acta 43A (1987) 1539–1542.
[21] G. Webb, Catal Today 7 (1990) 139–155.
[22] M. Tushaus, W. Berndt, H. Conrad, A. Bradshaw, B. Persson, Appl. Phys. A 51 (1990) 91–98.